EMPIRICAL ATMOSPHERE MODEL IN A MINI FLARE DURING MAGNETIC RECONNECTION

Brigitte Schmieder[1,2], Reetika Joshi[3], Ramesh Chandra[3],
Guillaume Aulanier[4], Akiko Tei[5], Petr Heinzel[6], James Tomin[1],
Nicole Vilmer[1], and Véronique Bommier[1]

[1] *LESIA, Observatoire de Paris, Université PSL, CNRS, Sorbonne Université,
Université de Paris, 5 place Jules Janssen, 92190 Meudon, France*
[2] *Centre for mathematical Plasma Astrophysics, Dept. of Mathematics,
KU Leuven, 3001 Leuven, Belgium*
[3] *Department of Physics, DSB Campus, Kumaun University,
Nainital-263001, India*
[4] *Laboratoire de Physique des Plasmas (LPP), École Polytechnique,
IP Paris, Sorbonne Université, CNRS, Observatoire de Paris,
Université PSL, Université Paris Saclay, Paris, France*
[5] *Institute of Space and Astronautical Science, Japan, Aerospace Exploration Agency,
3-1-1 Yoshinodai, Chuo-ku, Sagamihara, Kanagawa 252-5210, Japan*
[6] *Astronomical Institute of the Czech Academy of Sciences, Fričova 298, 251 65
Ondřejov, Czech Republic*

Abstract. A spatio-temporal analysis of IRIS spectra of MgII, CII, and SiIV ions allows us to study the dynamics and the stratification of the flare atmosphere along the line of sight during the magnetic reconnection phase at the jet base. Strong asymmetric MgII and CII line profiles with extended blue wings observed at the reconnection site are interpreted by the presence of two chromospheric temperature clouds: one explosive cloud with blueshifts at 290 km s^{-1} and one cloud with smaller Doppler shift (around 36 km s^{-1}). Simultaneously at the same location a mini flare was observed with strong emission in multi temperatures (AIA), in several spectral IRIS lines (e.g. OIV and SiIV, MgII), absorption of identified chromospheric lines in SiIV line profile, enhancement of the Balmer continuum and X-ray emission by FERMI/GBM. With the standard thick-target flare model we calculate the energy of non thermal electrons observed by FERMI and compare it to the energy radiated by the Balmer continuum emission. We show that the low energy input by non thermal electrons above 20 keV was still sufficient to produce the excess of Balmer continuum.

Key words: Solar jets - flares - magnetic reconnection

1. Introduction

Solar flare models have been extensively developed using 1D to 3D non LTE radiative transfer codes in flare loops (Allred et al., 2020; Kerr et al., 2020). The sites of chromospheric excitation during solar flares are marked by white light emission, extended extreme ultraviolet ribbons and hard X-ray footpoints. The standard interpretation is that these are the result of heating and bremsstrahlung emission from non-thermal electrons precipitating from the corona (Fletcher et al., 2013). Solar flare models interpret enhancements of emission in white light and in Balmer continuum by non thermal electron beams (Heinzel and Kleint, 2014; Kleint et al., 2016, 2017; Kowalski et al., 2017). It is important to understand the relationship between electron beams and radiative emission for interpreting white light super flares in stars (Kowalski et al., 2012; Heinzel and Shibata, 2018).

We report on a solar jet observed in multi wavelength with the *Interface Region Imaging Spectrograph* (IRIS, De Pontieu et al., 2014) (IRIS) in chromospheric lines and with the *Atmospheric Imaging Assembly* (AIA, Lemen et al., 2012) on board the *Solar Dynamics Observatory* (SDO, Pesnell et al., 2012) occurring on March 22 2019. This event has been well described using spectroscopy data of IRIS and spectropolarimetry data from HMI in a series of papers (Joshi et al., 2020; Joshi, Schmieder, Tei, Aulanier, Lörinčík, Chandra and Heinzel, 2021; Joshi, Schmieder, Heinzel, Tomin, Chandra and Vilmer, 2021) and NLFF extrapolation of the photosphere magnetic field have been performed (Yang et al., 2020).

Here we present a summary of the observations leading to an empirical atmosphere model of the mini flare at the base of the jet (UV burst). The mini flare (GOES B6.7) occurred in the active region (AR NOAA 12736), which was located at N09 W60 on March 22, 2019.

2. Observations

The AR was the only AR in the whole solar disk on that day (Fig. 1 panel a). The AR was formed during the day and the previous day, by successive emerging fluxes. At the time of the jet at 02:04 UT two emerging flux collapse and a flux rope was created between them (Joshi et al., 2020). Figure 1 panel (b) shows an AIA 304 image with overlying magnetic field contours which indicate the presence of positive and negative polarities on both side
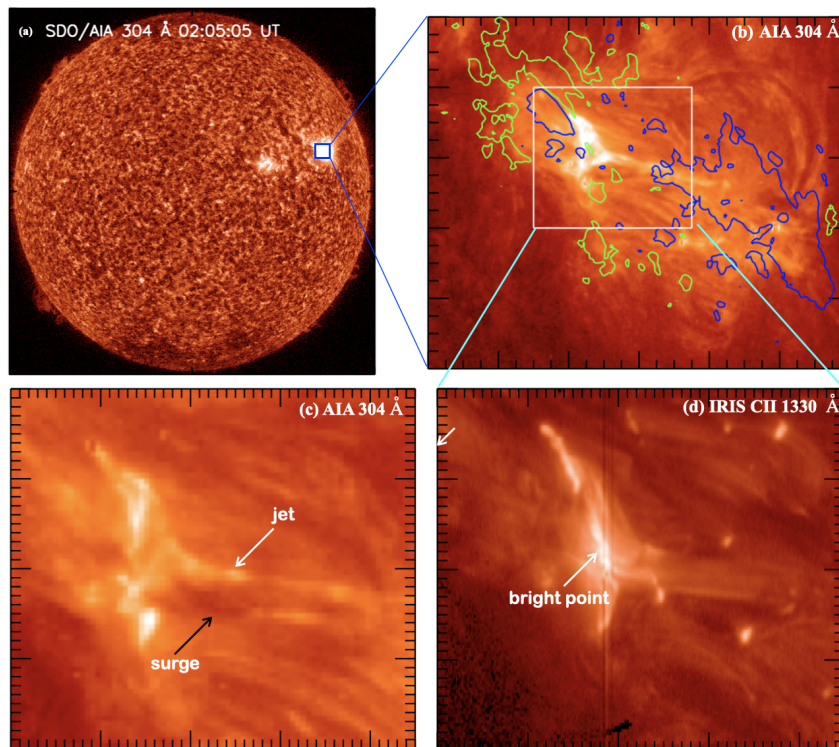
Figure 1: Observations of the solar jet and surge on March 22, 2019. Panel a shows the full disk image of the Sun, and the blue rectangular box is the AR zoomed in panel b. In panel b the green and blue contours represent positive and negative magnetic polarity respectively ($\pm$ 300 Gauss). Magnetic reconnection occurred between two emerging magnetic flux regions. The jet and cool surge are indicated in panel c. The reconnection site (bright point) is crossed by the IRIS slit position 1 indicated in panel d.

of the brightening. These polarities are squeezed and at the location of the bright arch center a small bipole (blue and green) is detected. The reconnection occurs at this point and a bright vault is observed from which escapes the jet. In panel (c) the bright jet and a parallel dark surge are observed. The bright point is indicated in panel (d). This bright point is observed in all the channels of AIA indicating that the plasma is heated to more than 1 MK and corresponds to the B 6.7 X-class detected by GOES.

IRIS spectra have been analysed showing the evolution of the jet and the mini flare at its base in the three band passes centered in MgII, CII and SiIV lines (Fig. 2). The spectra along the slit shows in all the panels at 02:04:28 UT an extended horizontal brightening, indicating large flows and heating. These flows are characterized as bidirectional flows during the
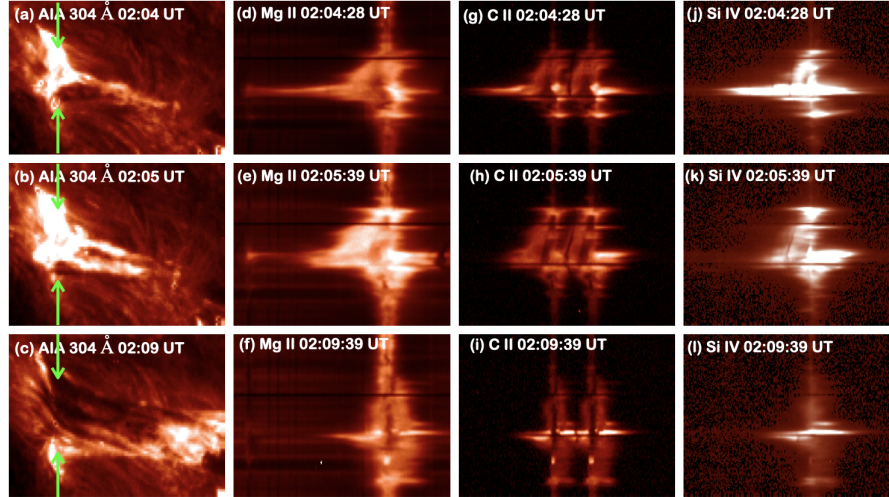
Figure 2: Jet reconnection base (UV burst/mini-flare) and jet evolution. First column: images in AIA 304 Å. Second, third, and last columns show IRIS spectra of the jet reconnection site at the slit position 1 (shown by green arrows).

reconnection. The extension of the flows have been calculated with the cloud model technique and two clouds were identified with flows of -36 km s^{-1} and -300 km s^{-1}. The brightening is also extended far away of Mg II k line blue wing indicating an enhancement of the Balmer continuum. The Balmer continuum presents an excess of brightness by 50%.

We combine the observations of Balmer continuum obtained with IRIS (spectra and SJI 2832 Å) and hard X-ray emission detected by FERMI Gamma Burst Monitor (GBM) during the reconnection producing the mini flare (Fig. 3). Calibrated Balmer continuum is compared to non-LTE radiative transfer flare models and radiated energy is estimated. With the standard thick-target flare model we calculate the energy of non-thermal electrons detected by FERMI GBM and compare it to the radiated energy (Joshi, Schmieder, Heinzel, Tomin, Chandra and Vilmer, 2021). We need to assume a very small area for the reconnection site, probably smaller then the IRIS pixel resolution for a satisfactory fit.

3.   Conclusion

From the study of the IRIS spectra and filter images we deduce an empirical flare model for the mini flare (UV burst) at the base of the jet during
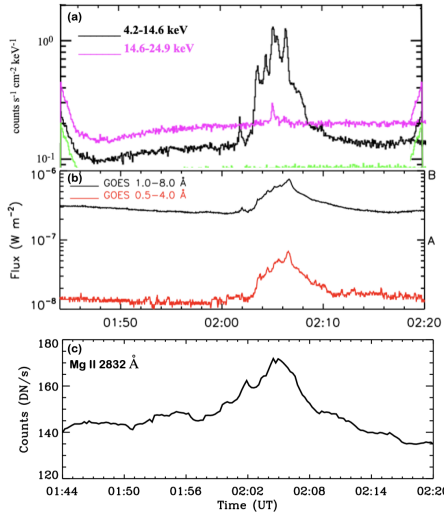
Figure 3: Hard X-ray emission recorded by FERMI/GBM (panel a), GOES soft X-ray (panel b), light curve of the intensity in the bright point in the Balmer continuum image obtained from the IRIS SJI at 2832 Å (panel c).
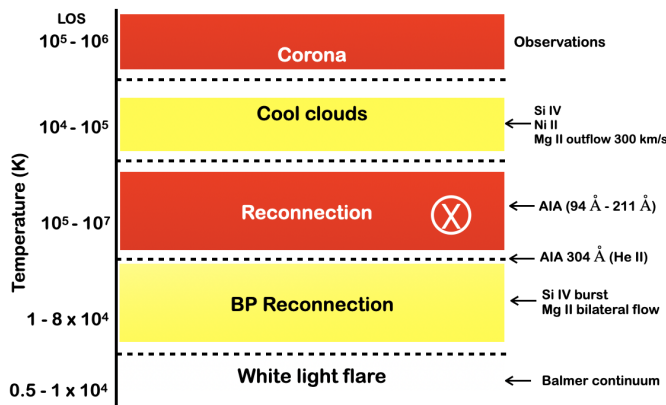

Figure 4: Empirical flare model along the line of sight (LOS) through the current sheet observed at the reconnection point deduced from the analysis of the IRIS spectra and AIA images.

reconnection (Fig. 4). A sandwich of different temperature layers explain the observations. It is consistent with MHD models (Hansteen et al., 2019).

References

Allred, J. C., Alaoui, M., Kowalski, A. F., and Kerr, G. S.: 2020, *Astrophys. J.* **902**(1), 16.

De Pontieu, B., Title, A. M., Lemen, J. R., Kushner, G. D., Akin, D. J., Allard, B., Berger, T., Boerner, P., Cheung, M., Chou, C., Drake, J. F., Duncan, D. W., Freeland, S., Heyman, G. F., Hoffman, C., Hurlburt, N. E., Lindgren, R. W., Mathur, D., Rehse, R., Sabolish, D., Seguin, R., Schrijver, C. J., Tarbell, T. D., Wülser, J.-P., Wolfson, C. J., Yanari, C., Mudge, J., Nguyen-Phuc, N., Timmons, R., van Bezooijen, R., Weingrod, I., Brookner, R., Butcher, G., Dougherty, B., Eder, J., Knagenhjelm, V., Larsen, S., Man-

sir, D., Phan, L., Boyle, P., Cheimets, P. N., DeLuca, E. E., Golub, L., Gates, R., Hertz, E., McKillop, S., Park, S., Perry, T., Podgorski, W. A., Reeves, K., Saar, S., Testa, P., Tian, H., Weber, M., Dunn, C., Eccles, S., Jaeggli, S. A., Kankelborg, C. C., Mashburn, K., Pust, N., Springer, L., Carvalho, R., Kleint, L., Marmie, J., Mazmanian, E., Pereira, T. M. D., Sawyer, S., Strong, J., Worden, S. P., Carlsson, M., Hansteen, V. H., Leenaarts, J., Wiesmann, M., Aloise, J., Chu, K.-C., Bush, R. I., Scherrer, P. H., Brekke, P., Martinez-Sykora, J., Lites, B. W., McIntosh, S. W., Uitenbroek, H., Okamoto, T. J., Gummin, M. A., Auker, G., Jerram, P., Pool, P., and Waltham, N.: 2014, *Sol. Phys.* **289**, 2733–2779.

Fletcher, L., Hannah, I. G., Hudson, H. S., and Innes, D. E.: 2013, *Astrophys. J.* **771**(2), 104.

Hansteen, V., Ortiz, A., Archontis, V., Carlsson, M., Pereira, T. M. D., and Bjørgen, J. P.: 2019, *Astron. Astrophys.* **626**, A33.

Heinzel, P., and Kleint, L.: 2014, *Astrophys. J., Lett.* **794**(2), L23.

Heinzel, P., and Shibata, K.: 2018, *Astrophys. J.* **859**(2), 143.

Joshi, R., Schmieder, B., Aulanier, G., Bommier, V., and Chandra, R.: 2020, *Astron. Astrophys.* **642**, A169.

Joshi, R., Schmieder, B., Heinzel, P., Tomin, J., Chandra, R., and Vilmer, N.: 2021, *Astron. Astrophys.* **654**, A31.

Joshi, R., Schmieder, B., Tei, A., Aulanier, G., Lörinčík, J., Chandra, R., and Heinzel, P.: 2021, *Astron. Astrophys.* **645**, A80.

Kerr, G. S., Allred, J. C., and Polito, V.: 2020, *Astrophys. J.* **900**(1), 18.

Kleint, L., Heinzel, P., Judge, P., and Krucker, S.: 2016, *Astrophys. J.* **816**(2), 88.

Kleint, L., Heinzel, P., and Krucker, S.: 2017, *Astrophys. J.* **837**(2), 160.

Kowalski, A. F., Allred, J. C., Daw, A., Cauzzi, G., and Carlsson, M.: 2017, *Astrophys. J.* **836**(1), 12.

Kowalski, A. F., Hawley, S. L., Holtzman, J. A., Wisniewski, J. P., and Hilton, E. J.: 2012, *Sol. Phys.* **277**(1), 21–29.

Lemen, J. R., Title, A. M., Akin, D. J., Boerner, P. F., Chou, C., Drake, J. F., Duncan, D. W., Edwards, C. G., Friedlaender, F. M., Heyman, G. F., Hurlburt, N. E., Katz, N. L., Kushner, G. D., Levay, M., Lindgren, R. W., Mathur, D. P., McFeaters, E. L., Mitchell, S., Rehse, R. A., Schrijver, C. J., Springer, L. A., Stern, R. A., Tarbell, T. D., Wuelser, J.-P., Wolfson, C. J., Yanari, C., Bookbinder, J. A., Cheimets, P. N., Caldwell, D., Deluca, E. E., Gates, R., Golub, L., Park, S., Podgorski, W. A., Bush, R. I., Scherrer, P. H., Gummin, M. A., Smith, P., Auker, G., Jerram, P., Pool, P., Soufli, R., Windt, D. L., Beardsley, S., Clapp, M., Lang, J., and Waltham, N.: 2012, *Sol. Phys.* **275**, 17–40.

Pesnell, W. D., Thompson, B. J., and Chamberlin, P. C.: 2012, *Sol. Phys.* **275**, 3–15.

Yang, S., Zhang, Q., Xu, Z., Zhang, J., Zhong, Z., and Guo, Y.: 2020, *arXiv e-prints* p. arXiv:2005.09613.